Rapid Communication in Photoscience(2013), vol. 2, no. 1, pp.9-17 ISSN 2234-8182
http://dx.doi.org/10.5857/RCP.2013.2.1.009

Review article

Single Nanoparticle Photoluminescence Studies of Visible Light-Sensitive TiO_2 and ZnO Nanostructures

Minjoong Yoon*

Molecular/Nano Photochemistry & Photonics Lab, Department of Chemistry, Chungnam National University, 79 Daehak-ro, Yuseong-gu, Daejeon, 305-764, Republic of Korea

ABSTRACT Visible light-sensitive TiO_2 and ZnO nanostructure materials have attracted great attention as the promising material for solar energy conversion systems such as photocatalysts for water splitting and environmental purification as well as nano-biosensors. Success of their applications relies on how to control their surface state behaviors related to the exciton dynamics and optoelectronic properties. In this paper, we briefly review some recent works on single nanoparticle photoluminescence (PL) technique and its application to observation of their surface state behaviors which are raveled by the conventional ensemble-averaged spectroscopic techniques. This review provides an opportunity to understand the temporal and spatial heterogeneities within an individual nanostructure, allowing for the potential use of single-nanoparticle approaches in studies of their photoenergy conversion and nano-scale optical biosensing.

INTRODUCTION

TiO_2 and ZnO nanomaterials have been attracting a great deal of attention due to their photocatalytic applications for degradation of organic pollutants,[1-3] artificial photosynthetic systems useful for solar energy conversion,[4,5] nano-bio applications[6,7] etc. Such applications are based on photoinduced generation of electrons and holes (excitons) at their surface. However, most of the semiconductor nanomaterials, particularly zero dimensional nanoparticles have two drawbacks for the wider applications. One is that they have wide band gap energy corresponding to UV light energy so that they have limitations to harvest visible light for solar energy conversion or nano-bio application. The other drawback is that the charge separation required for efficient redox reaction for the photocatalytic application is in competition with fast e-h recombination to form the luminescent exciton states required for the nano-bio application. Thus, it has been interesting subject how one can obtain the visible light-sensitive TiO_2 and ZnO nanomaterials and how the exciton dynamics can be controlled depending on the applications.

***To whom correspondence should be addressed.**
E-mail: mjyoon@cnu.ac.kr

The exciton dynamics of the zero dimensional nanoparticles are known to be controlled by manipulation of their particle sizes. As the particle size (diameter) is smaller than the thickness of space charge layer, the surface area becomes larger, and the charge separation becomes effective to retard the e-h recombination.[8,9] However, the ultrafine nanoparticles have a tendency to agglomerate into larger particles in practical use,[10, 11] resulting in adverse effect on the exciton dynamics. Also the size reduction of the nanoparticles remains limit to improve the visible light sensitivity because of the quantum confinement effect. Therefore, to solve these problems, there have been many attempts to modify the surface state characteristics such as surface state density and electron/hole trapping kinetics by decreasing the degree of overlap of the electron and hole wave functions by synthesizing 1- or 2-dimensional single-crystalline nanostructures such as nanotubes (NTs),[12-14] nanowires (NWs) and nanodiscs (NDs).[15] In the nanostructures, the photoinduced electron transfer is speculated to be facilitated through the surface layer because of high aspect ratio and large surface area reducing inter-crystalline contacts of TiO_2 or ZnO.

The surface optoelectronic properties of such nanostructures including the exciton dynamics of the nanostructures have been mostly investigated using ensemble-averaged laser spectroscopic techniques including diffuse reflectance transient absorption spectroscopy[16-18] and time-resolved photoluminescence (PL) spectroscopy[19, 20] from femtosecond to millisecond time scale as well as steady state PL spectroscopy.

However, the ensemble-averaged spectral techniques are performed on the ensemble-average basis of the inhomogeneous particle size and morphology distribution of nanoparticles, which presumably cause the inhomogeneous particle-surface and particle-particle interactions and inhomogeneous exciton dynamics. Thus, they have limitations in unequivocal assignment of the exciton-trapped surface states, differentiation of the particle size effects from the surface-state density effects on the exciton dynamics as well as the optical properties of the nanostructures. Also the conventional spectral techniques use high power of excitation light source (0.5 mJ~5 mJ) so that unexpected surface photochemistry takes place to misjudge the photophysical data. Therefore, in order to solve these problems, it is necessary to probe individual nanostructure behaviors hidden within the uncorrelated ensemble systems by using single nanoparticle spectroscopic techniques similar to single molecule spectroscopy.[21, 22]

Since Bawendi *et al.* reported the first observation of the unique PL intermittency from a single ZnS-overcoated CdSe QDs,[23] the single nanoparticle spectroscopy has been applied to study the surface state behaviors including exciton dynamics of different single semiconductor QDs such as ZnS-overcoated CdS, and CdTe,[24-27] InGaAs/GaAs[28] and $Y_2O_2S:Eu^{3+}$ QDs.[29] Such investigations have yielded the statistics of PL switching events between bright ("on") and dark ("off") state (blinking).[23] There have been various models proposed for blinking mechanisms in the QDs. Figure 1 shows a commonly accepted model of the blinking events in the II-VI colloidal QDs was firstly suggested by Efros and Rosen.[30] It is based on a long-lived trap hypothesis that PL is quenched by trapping of the exciton pair in the long-lived surrounding matrix (*e.g.* ZnS) and consequent Auger ionization. In the ionized QDs, the exciton pair an be recombined by an ultrafast radiationless Auger process (1 ps).[25]

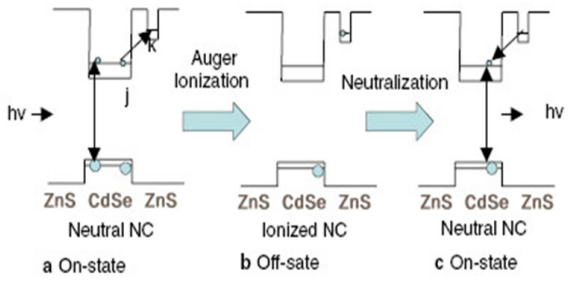

Figure 1 Auger ionization mechanism for the blinking PL from a single QD. This is modified from ref. 27.

That is, the PL switching events are connected with the electron transitions from the QD to the long-lived trap site. This mechanism has been supported by several experiments[31, 32] and theoretical calculations.[27] The blinking periods are known to exhibit power-law statistics in the form of probability densities, ρ (t) $\sim t^{-(1+\upsilon)}$ where υ: 0.4~1.0. More advanced explanations of the power law distribution of "off" times were attempted using a wide range of exponentially distributed ionization-recombination rates, switched randomly after each electron transition between the QD states and the surrounding multiple electron traps.[33] The electron transfer event switching the PL intensity was proposed to happen only when the excited state and trap state are in resonance, providing a concept of a slow diffusive coordinate which explains the large difference between excitation-relaxation times of electronic states of the QD and the blinking times.[34] This proposition was improved by Tang and Marcus[35] and Margolin *et a.,*[36] explaining the PL blinking caused by three dimensional hopping diffusion of the photoejected electron into the surrounding trapping media. The ionized QD stays "off", while the QD stays "on" as long as the electron diffusing with the hole trapped. However, this model cannot explain the escape of the trapped electron such as the interfacial electron transfer.

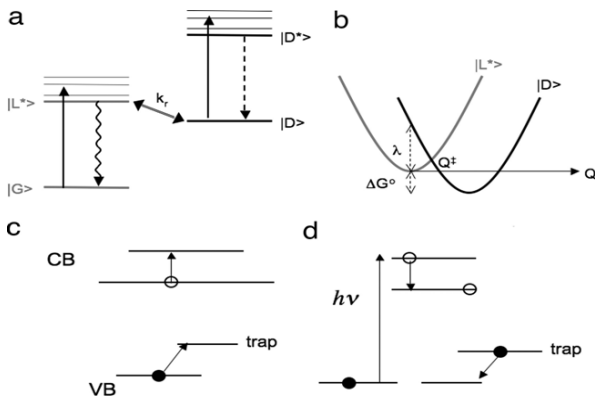

Figure 2 Diffusion-controlled electron transfer (DCET) model for PL blinking of QD. This is modified from ref. 38.

Thus, Frantsuzov and Marcus[37] proposed alternative model without the long-lived trap hypothesis, and Pelton and Marcus *et al.* verified it by characterizing the blinking fluctuations of ZnS/CdSe QDs over time scales from milliseconds to seconds.[38] According to their model, the PL intermittency of QD is caused by large variations of the radiationless relaxation rates of

the excited electronic state to the ground state *via* the hole trap states induced by an Auger-assisted hole trapping to the deep surface states, which is accompanied by the simultaneous electron excitation to the higher electronic states beyond the conduction band as shown in Figure 3. They found that the PL blinking is controlled by diffusion of the energies of electron or hole trap states as a function of the nuclear coordinates of the system. Thus, blinking PL studies of the single semiconductor nanoparticles would be very useful for analysis of electron or hole transfer movements on the surface states.

However, the exciton recombination in the naked QDs without the surrounding matrix (ZnS) as a long-lived trap is too fast to exhibit the PL intermittency, and it would be interesting to modify the QDs into low dimensional nanostructures or composites which facilitate the electron-hole separation. Recently, Glennon *et al.*[39, 40] observed PL blinking of one dimensional CdSe quantum wires, the mechanism of which was suggested to be different from that commonly explained for the PL blinking of semiconductor QDs, presenting a simple surface-trap-filling model based on the dynamic, transient filling of surface-trap sites by excitons and the emptying the occupied trap sites.

Herein, a few example of application of the single nanoparticle PL spectroscopy to visible light-sensitive TiO_2 or ZnO nanostructures and composites are briefly reviewed with regard to their optoelectronic properties including exciton dynamics. This review provides information of single nanoparticle approach for estimation of the photoenergy conversion and the nano-bio applications of the semiconductor nanostructures and composites.

INSTRUMENTATION

The images and PL spectral properties of single nanoparticle or nanostructures can be measured at room temperature by using LSCM-coupled ps-time-resolved PL system[41] (Figure 3). The samples-coated cover slide glass on a scanning piezo-electric X-Y stage (Physik Instrumente, P517.3CL) is illuminated with 405 nm light (10 μW cm^{-2}) from CW diode laser (NEO ARK, LDT-4005) or second harmonic generated self-mode-locked Ti:sapphire laser (Coherent model Mira 900) (390 nm) pumped by a Nd :YVO_4 laser (Coherent Verdi diode pumped laser) (200 fs pulse width with repetition rate of 76 MHz) for PL images, steady-state and time-resolved spectral measurements, respectively. This light is passing through the single mode optic fiber and then incident on the back of a 100 × 1.3 NA oil immersion objective lens (Carl Zeiss Plan-NEOfluor). The PL signals are collected through an inverted confocal scanning microscope (Carl Zeiss Axiovert 200). The emission is isolated from Rayleigh scattering by a combination of filters, an excitation filter BP 395-440, a dichroic filter FT 460 and an emission filter LP 470 (Carl Zeiss).

The PL images of the single nanostructures are obtained through detection of epiluminescence over a focused laser spot of 300 nm diameter by using a liquid nitrogen-cooled and intensified charge-coupled device (CCD) detector (Princeton Instruments VersArray) *via* single-photon counting avalanche photodiode (Perkin-Elmer SPCM-AQR-13FC) with wide-field excitation in a similar way to the single molecule PL detection.[42] The chip of the CCD has a total active area of 12.3 × 12.3 mm divided into 512 × 512 pixels (size: 24 × 24 μm), which is operated at −110 °C. The wide-field images were acquired with the software WinSpec (Princeton Instruments).

The PL spectra of a single nanoparticle selected from the PL image of several nanoparticles are obtained with accumulation of emissive photons within 200 ms per spectrum at room temperature by a polychromator (Acton Research, Spectra Pro 300i) with a charge coupled device (CCD) camera (Roper Scientific, PI-MAX-1024HG18) *via* optical fiber. The excitation wavelength is 405 nm.

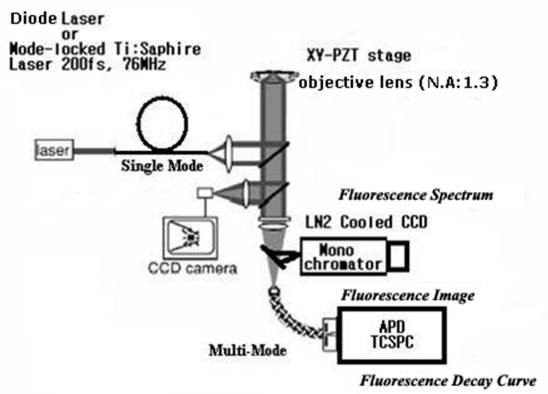

Figure 3 Schematic layout of the laser scanning confocal microscope (LSCM)-coupled steady-state and ps-time-resolved PL system

OPTOELECTRONIC PROPERTIES OF VISIBLE LIGHT-SENSITIVE SINGLE TiO_2 NANODICS (NDs)

Figure 4 shows TEM and AFM images of two-dimensional TiO_2 NDs synthesized by sol-gel method through formation of liposome-TiO_2 nanocomposites using egg-lecithin lipid as a template as previously established.[15] The TiO_2 NDs are anatase nanocrystals as seen from the well-defined SAED and 0.35nm lattice spacing (Figure 4(A) inset) with the

average diameter of 9 nm and central height of ~2nm as determined from the cross sectional analysis of the AFM images. Figure 4 (C) shows the ensemble-averaged diffuse reflectance fluorescence emission (b) and excitation spectra of TiO_2 NDs on slide glass, being attributed to recombination of electron-hole on multiple surface states for visible light absorption beyond 400 nm.

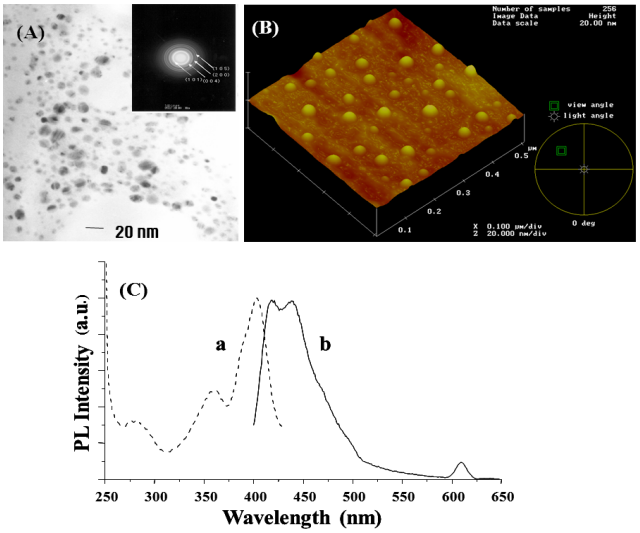

Figure 4 (A) TEM images of TiO_2 NDs showing anatase SAED (Inset). (B) AFM images of TiO_2 NDs on quartz slide glass measured by tapping mode. (C) The ensemble-averaged PL excitation (a) and emission (b) spectra of TiO_2 NDs measured at ambient temperature. The excitation wavelength for the emission spectrum was 360 nm, and the emission wavelength for the excitation spectrum was 440 nm. These results are reported in ref. 43.

The individual TiO_2 NDs show the strong PL emission images as seen from the AFM images, exhibiting blinking behaviors (Figure 5(left)). Analysis of the PL blinking time trajectories (Figure 5 (right)) revealed single-exponential kinetics with the average lifetimes of on-state (τ_{on} ~286ms) and off-state (τ_{off} ~58ms), implying that the blinking is due to a single process, interfacial electron transfer to the $_4Ti^{4+}$ −OH surface trap sites with the simultaneous Auger-assisted hole trapping by alternative trapping and detrapping of excitons through multiple surface states(Figure 6A) similarly to the diffusive coordinate model proposed by Frantsuzov and Marcus.[36]

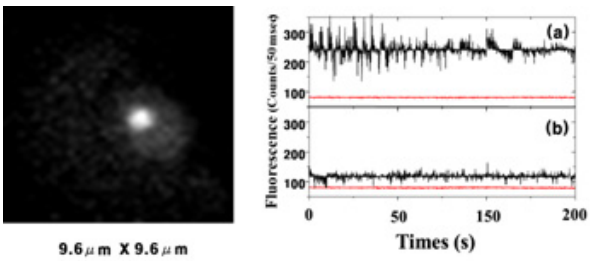

Figure 5 (Left) Blinking PL images of TiO_2 NDs (Right) Time-dependent trajectories of PL intensities for one representative single TiO_2 ND (a) and TiO_2 QD (b). The bottom traces (red color) are the non-luminescent background noise levels measured from the slide glass without TiO_2 nanoparticles. Mean noise amplitudes: ±40counts. Binning time: 50 ms; Excitation light power fluctuation < 10%. These results are reported in ref. 43.

The switcher of PL with the electron trapping and interfacial electron transfer to the surface trap site is described in terms of energy transformation as shown in Fig. 6B. In accordance with the diagram shown in Fig. 6B, the rate of the back electron transfer (k_{bet}) corresponding to trapping into the surface states from the surface trap site is simply the inverse of the average lifetimes of the off-state (τ_{off}) as equation (1). On the other hand, the decay rate of the on-state ($1/\tau_{on}$) depends on the excitation rate (k_{exc}) and PL decay rate (k_r) of

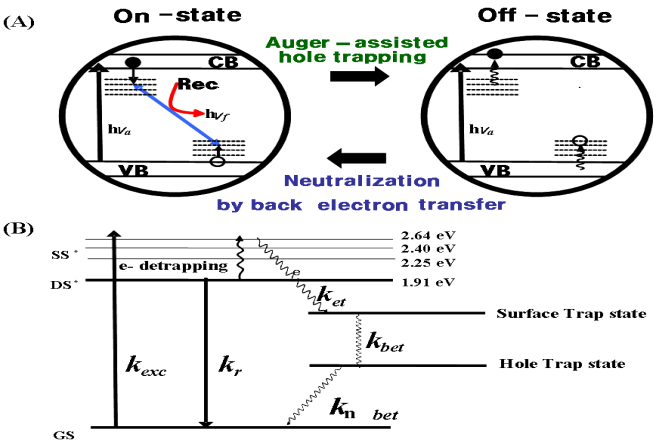

Figure 6 (A) Ionization/neutralization process through electron trapping (tr) and detrapping (dep) in TiO_2 ND under laser illumination, forming PL on-state and off-state. Rec stands for surface trap-site and recombination. (B) Energy transformation model for the switcher of PL with the electron detrapping and interfacial electron transfer to the surface trap state for TiO_2 ND whose PL displays blinking behavior. Once

the electron is transferred back to the hole trap state, very fast radiationless relaxation (k_n) would take place. These results are reported in ref. 43.

The exciton states which correspond to the e–h recombination rate, as well as the rate of interfacial electron transfer (k_{et}) as in equation (2).[27]

$$\frac{1}{\tau_{off}} = k_{bet} \quad (1)$$

$$\frac{1}{\tau_{on}} = k_{exc}\frac{k_{et}}{k_r + k_{et} + k_{exc}} \quad (2)$$

Thus, the rates of forward and backward interfacial electron transfer can be readily determined by using these two equations with k_{exc} and k_r, where k_{exc} is estimated by taking power (10 μW cm^{-2}) of 390 nm laser and absorption cross sections of ND, σ_{ND} = 7.9 × 10^{-13} cm^2 and k_r is the inverse of average luminescent decay time of the surface emission at 550 nm. In this particular case, the rates of the forward and backward interfacial electron transfer calculated are 18ns and 58ms, respectively, which are slow enough to keep the polarization of e-h pairs at surface for efficient photocatalysis and photovoltaic activities. The present methodology and results would be useful to obtain surface exciton dynamics of other photoelectronic semiconductor nanostructures.

OPTOELECTRONIC PROPERTIES OF Sn-PORPHYRIN-INTERCALATED TiO_2 NANOFIBERS

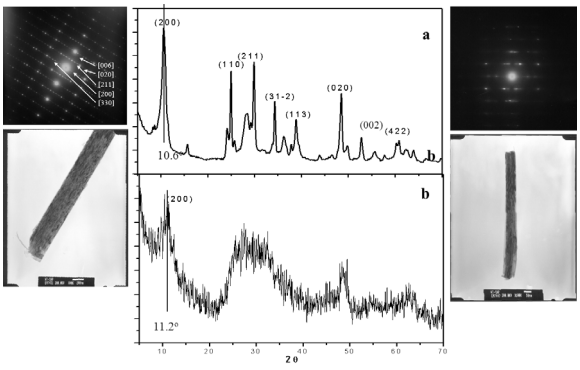

Figure 7 X-ray diffraction patterns of SnTTP-TiNF (a) and free TiNF (b) with TEM and SAED images of SnTTP-TiNFs. These results are reported in ref 44.

The single nanoparticle spectroscopy was applied to a new class of nanostructural composites, Sn-porphyrin-intercalated TiO_2 nanofibers (SnTTP-TiNF) fabricated by one-step hydrothermal reaction of a mixture solution of TiO_2 anatase powder and a Sn-porphyrin, *trans*-dihydroxo[5,10,15,20]-tetrakis(*p*-tolyl) porphyrinato]tin(IV) [SnTTP], which are well-crystalline trititanate ($H_2Ti_3O_7$)-type multilayered nanofibers (TiNFs) with lengths in the range of 0.5－1 μm with an average diameter of approximately 50 nm as confirmed by TEM and SAED images with XRD patterns as seen from Figure 7.[44]

Figure 8 shows the diffuse reflectance UV-visible absorption spectrum of SnTTP-TiNFs compared with those of free SnTTP powders and aqueous solution, exhibiting band broadening as compared to those of the monomer bands and the condensed solid state of SnTTP. The band broadening of the nanofibers may be due to the coherent coupling of the transition dipoles of porphyrin molecules through coplanar interaction in parallel with trititanate layers. If that is the case, such aggregate type may be beneficial to induce a cascade of the photoinduced electrons from the parallel trititanate layers, causing an efficient polarized electron transfer without photo-damage of the porphyrin aggregates.

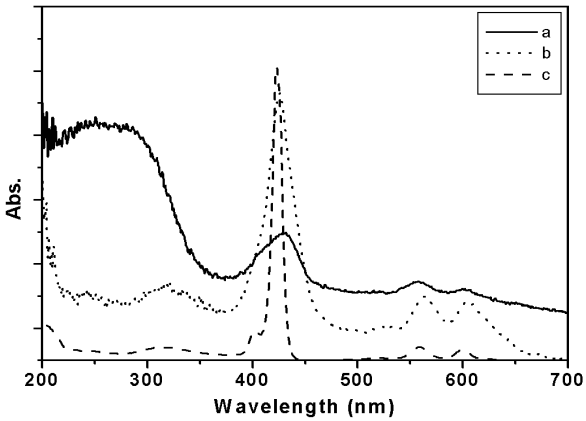

Figure 8 Diffuse reflectance UV-visible absorption spectra of SnTTP-TiNFs (a) and SnTTP powders (b). The absorption spectrum of diluted aqueous solution of SnTTP (5.0 x 10^{-6} M) corresponding to that of SnTTP monomer (c). These results are reported in ref. 44.

Supporting this speculation, the ensemble-averaged PL emission spectrum of the aqueous dispersion of SnTTP－TiNFs was observed to be quenched as compared to that of free TiNFs. However, free TiNFs exhibit broad surface emission bands which are overlapped with those of SnTTP and TiNFs, and it is difficult to clarify the pathway of the photoinduced electron transfer in SnTTP-TiNFs. Thus, the single nanoparticle PL of a free TiNF was measured as shown in Figure 9, which shows clear surface

emission bands while SnTTP-TiNF exhibits the deep surface emission at 650 nm with excitation at 405 nm. These results indicate that the photoinduced electrons are trapped in the deep surface states, followed efficiently transferred to the intercalated SnTTP, forming an anion radical $SnTTP^{\bullet-}$ which is known to be nonfluorescent,[45] These results also suggest that recombination of electron and hole pairs produced from trititanate is inhibited by SnTTP.

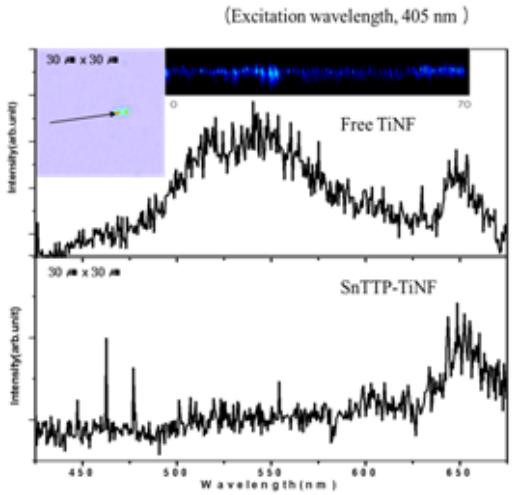

Figure 9 Single nanoparticle PL emission spectra of SnTTP-TiNF and free TiNF. Inset: PL image of a single free TiNF (left) and time-dependent trajectories of PL intensities for one representative single TiNF (right). These results are reported in ref. 44.

OPTOELECTRONIC PROPERTIES OF VISIBLE LIGHT-SENSITIVE ZnO NANOWIRES: WAVEGUIDE PROPERTIES

One-dimensional ZnO nanostructures such as ZnO nanowires, nanorods and nanobelts have received considerable attention due to their unique optoelectronic properties (light-sensitive changes of surface polarity and electron transport),[46] and they have been applied to photochemical sensors[47] and photonic devices (nano-lasers and LED).[48-50] Also ZnO is biocompatible, and nontoxic, and the ZnO nanostructures have been applied to develop biosensor (high iso-electric point (9.5) for easy immobilization of DNA or proteins).[6, 7] However, such biosensor application is based on electric properties of ZnO but not on the optical properties. This is because ZnO absorbs bio-hazard UV light corresponding to its wide band gap energy of 3.37 eV.

Further, the optoelectronic properties of ZnO nanostructures have been mostly explored by UV excitation only, and there have been limitations to understand them unambiguously. For example, upon UV excitation, ZnO nanowires exhibit two distinct emission bands: one is UV emission band (near 385 nm), the other is green emission band (near 510 nm) which are generally attributed to the direct exciton recombination on near band edge and small defect (oxygen and zinc vacancies) energy states, respectively. Particularly, the UV emission of a single ZnO nanowire has been reported to show strong waveguide mode peaks.[47] Excitation power stronger than a certain threshold allows UV lasing action to occur at room temperature. On the other hand, no wave guiding and laser actions are observed from the green emission. This fact has been postulated to be due to a decrease in the density of defects by increased exciton migration from the band edge to lower energy-defect state with the higher UV energy excitation.[50] However, question remains what if the defect states of ZnO nanostructures are directly excited with visible light. In order to answer this question as well as the expansion of optoelectronic application region from UV to visible wavelengths, visible light-dependent optoelectronic properties of the ZnO nanostructures need to be investigated.

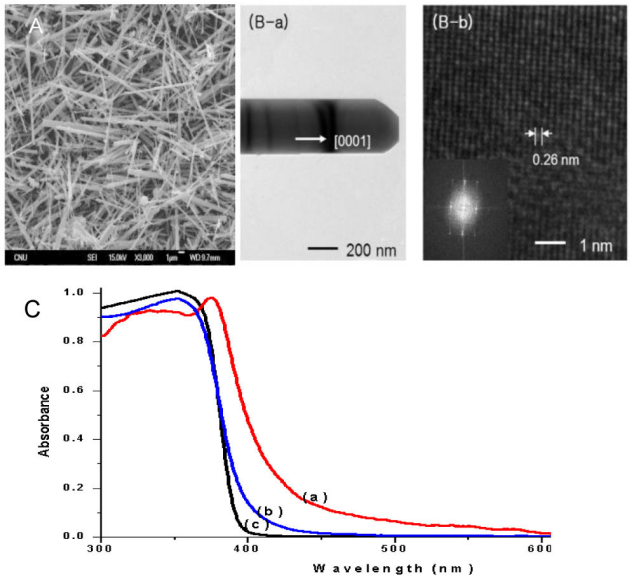

Figure 10 (A) SEM images of ZnO nanowires, (B) TEM image and high-resolution TEM image showing the lattice image of a ZnO nanowire (lattice spacing ~0.26nm). Inset: Fast Fourier transform (FFT) of the corresponding structures, and (C) diffuse reflectance absorption spectrum of ZnO nanowires (a) compared with those of ZnO nanorods (b) and ZnO nanoparticles. These results are reported in ref. 51.

Figure 10 (A) and (B) show the SEM and TEM images of ZnO nanowires synthesized by a modified sol-gel method through formation of liposome-ZnO nanocomposites with hydrothermal reaction,[51] which can absorb whole visible light as approved by the diffuse reflectance absorption spectrum (Figure 10 (C). The ZnO nanowires are Wurtzite single crystalline having aspect ratio of 7.5~50 with about 400 nm in diameter and 3~20 μm in length.

Figure 11 (a) shows PL images of individual ZnO nanowires measured upon excitation with visible light at 415 nm using the laser scanning confocal microscope (LSCM)-coupled PL system, exhibiting bright red emission at the tips with relatively weaker emission from the bodies. It is noteworthy that this unique PL behavior is not observed by UV excitation as reported by Yang's group.[47]This result implies that the as-prepared nanowire has visible light-sensitive waveguide properties of red emission, which have not been observed from the conventional ZnO nanowires. Supporting this, the single nanoparticle emission spectrum measured from the tip of the representative single nanowire (Figure 11(b)) shows definitely the periodical intensity variations (Figure 11(c) corresponding to waveguide mode peaks which are observed from the body (Figure 11(d). Also the tip emission was reported to prefer for the polarization along the wire major axis oriented at zero degree as seen from the polarization map of the emission intensity.[4] From the mode spacing of the red emission measured from 11 different nanowires of different lengths, the waveguiding behavior was analyzed to fit to Fabry-Perot equation, $\triangle\lambda=(\lambda^2/2L)[n-\lambda(dn/d\lambda)]^{-1}$ where $\triangle\lambda$: mode spacing, n: refractive index, $dn/d\lambda$: dispersion relation. Assuming $\lambda(dn/d\lambda)$~1.0 (*J. Appl. Phys.* **86** (1999) 408),with the slope, 2.24, n was determined to be 2.2. The red emission intensity was also found to be linearly depending on the excitation pump power, indicating that the density of defects would not be decreased by the exciton migrations as long as the defects are not disturbed by higher energy excitation with UV as predicted by Yang's group.[47] Such visible light-dependent optoelectronic behavior of the single ZnO nanowire may be useful for future sub-wavelength lasing cavity and visible light sensitive optoelectronic nanodevices, probably including optical nano-biosensor to detect biomolecule on nanoscale in a single cell using the single nanoparticle PL spectroscopic technique. Supporting this possibility, very recently in our lab, the tip emission of the single ZnO nanowire was found to be increased upon functionalization with DNA having selected base sequences whereas the body emission was little changed.[52]

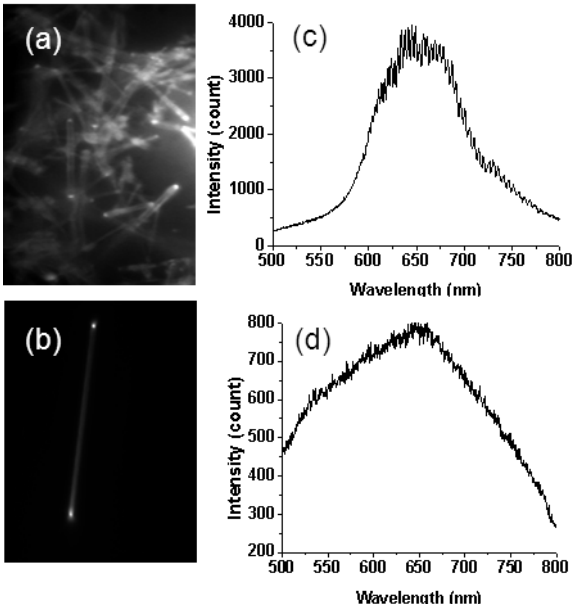

Figure 11 Single nanoparticle PL spectral properties of single ZnO Nanowires. (a) Epi-PL images of single ZnO nanowires, (b) a representative image of selected single ZnO nanowire, and emission spectrum collected from the tip (c) or body (d) of the selected single ZnO nanowire upon excitation with visible light at 415nm. These results are reported in ref. 51.

CONCLUSIONS

In this review, the single nanoparticle PL technique for evaluating surface state behaviors of semiconductor nanoparticles is featured by reviewing a few example of its application to visible light-sensitive TiO_2 or ZnO nanostructures and composites. Particularly, it is recognized that the single nanoparticle PL technique can provide good methodologies to estimate morphology-dependent exciton dynamics and interfacial electron transfer kinetics through analysis of PL blinking without the raveled problems such as inhomogeneous dynamics due to particle-surface and particle-particle interactions involved in the conventional ensemble-averaged laser spectroscopic techniques. Also it is useful to estimate the waveguide properties of the visible light-sensitive semiconductor nanostructures. Consequently the single nanoparticle PL technique combined with fabrication technique of visible light-sensitive TiO_2 or ZnO nanostructures would be very useful for design and development of efficient solar energy conversion nanostructures and optical nano-biosensors.

ACKNOWLEDGEMENTS

This study was financially supported by research fund of Chungnam National University in 2011, the National Research Foundation of Korea (Project number: NRF-2010-0002880; NRF-2012R1A1A 2039168) and the Brain Korea 21 (BK21) program of the Korea Ministry of Education

KEYWORDS: Single nanoparticle spectroscopy, Photo-luminescence, Visible light-sensitive semiconductor nanostructures, Photocatalysis, Nano-biosensors, Photoenergy conversion.

Received March 8, 2013; Accepted April 15, 2013

REFERENCES AND NOTES

1. Fujishima, A.; Rao, T.N.; Tryk, D.A. *J. Photochem. Photobiol. C,* **2000**, *1*, 1.
2. Li, Q.; Xie, R. C.; Li, Y. W.; Mintz, E. A.; Shang, J. K. *Environ. Sci. Technol.*, **2007**, *41*, 5050.
3. Chen, X.; Mao, S.S. *Chem.Rev.,***2007***,107,* 2891.
4. Yoon, M.; Chang, J. A.; Kim, Y.; Choi, J. R.; Kim, K.; Lee, S. J. *J. Phys. Chem. B*, **2001**, *105*, 2539.
5. Khan, S.; Al-Shahry, M.; Ingler, W. *Science*, **2002**, *297*, 2243.
6. Li, Z.; Yang, R.; Yu, M.; Bai, F.; Li, C.; Wang, Z. L. *J. Phys. Chem. C* **2008**,*112*,20114.
7. Liu, J.; Guo, C.; Li, C. M.; Li, Y.; Chi, Q.; Huang, X.; Liao, L.; Yu, T. *Electrochem. Commun.* **2009**, *11*, 202.
8. Chen, W. in *Handbook of Nanostructured Materials and Nano-technology*, ed. H. S. Nalwa, Academic Press, New York, USA, 2000, vol. 4 Chapter 5.
9. Wang, Y.; Herron, N. *J. Phys. Chem.*, **1991**, *95*, 525.
10. Zhang, X.; Yin, L.; Tang, M.; Pu, Y. *J. Nanosci. Nanotechnol.* **2010**, *10*, 8.
11. Suttiponparnit, K.; Jiang, J.; Sahu, M. Suvachittanonat, S.; Charunpanitkul, T.; Biswas, P. *Nanoscale Res. Lett.* **2011**, *6*. 27.
12. Adachi, M.; Murata, Y.; Harada, M.; Yoshikawa, S. *Chem. Lett.*, **2000**, 942. .
13. Chen, Q.; Du, G. H.; Zhang, S.; Peng, L.-M. *Acta Crystallogr., Sect. B*, **2002**, *58,* 587.
14. Jang, J. H.; Jeon, K. S.; Park, T. S.; Lee, K. W.; Yoon, M. *J. Chin. Chem. Soc.*, **2006**, *53*, 123.
15. Yoon, M.; Seo, M.; Jeong, C.; Jang, J. H.; Jeon, K. S. *Chem. Mater.*, **2005**, *17*, 6069.
16. Furube, A.; Asahi, T.; Masuhara, H.; Yamashita, H.; Anpo, M. *Chem. Lett.*, **1997**, 735.
17. Furube, A.; Asahi, T.; Masuhara, H.; Yamashita, H.; Anpo, M. *J. Phys. Chem. B*, **1999**, *103*, 3120.
18. Yoshihara, T.; Katoh, R.; Furube, A.; Tamaki, Y.; Murai, M.; Hara, K.; Murata, S.; Arakawa, H.; Tachiya, M. *J. Phys. Chem. B*, **2004**, *108*, 3817.
19. Amtout, A.; Leoneli, R. *Solid State Commun.*, **1992**, *84*, 349.
20. Fujihara, K.; Izumi, S.; Ohno, T.; Matsumura, M. *J. Photochem. Photobiol., A*, **2000**, 132, 99.
21. Hussels, M.; Konrad, A.; Brecht, M. *Rev. Scientific Instrumenents* **2012**, *83*, 123706/1.
22. Lebold, T.; Michaelis, J.; Bein, T.; Braeuchle, C. In *Characteriza-tion of Solid Materials and Heterogeneous Catalysts* (Ed. by Che, M.; Vedrine, J. C.) **2012**,***1***,585-607.
23. Nirmal, M.; Dabbousi, B. O.; Bawendi, M. G.; Macklin, J. J.; Trautman, J. K.; Harris, T. D.; Brus, L. E. *Nature*, **1996,** *383*, 802.
24. Neuhauser, R. G.; Shimizu, K. T.; Woo, W. K.; Empedocles, S. A. Bawendi, M. G. *Phys. Rev. Lett.*, **2000**, *85*, 3301.
25. Sugishaki, M.; Ren, H.-W.; Nishi, K.; Masumoto, Y. *Phys. Rev. Lett.*, **2001**, *86*, 4883.
26. Fisher, B. R.; Eisler, H.-J.; Stott, N. E.; Bawendi, M. G. *J. Phys. Chem. B*, **2004**, *108*, 143.
27. Osad'ko, I. S. *Chem. Phys.*, **2005,** *316*, 99.
28. Wang, X. Y.; Ma, W. Q.; Zhang, J. Y.; Salamo, G. J.; Xiao, M.; Shih, C. K. *Nano Lett.*, **2005**, *5*, 1873.
29. Nakkiran, A.; Thirumalai, J.; Jagannathan, R. Chem. Phys. Lett., **2007**, *436*, 155.
30. Efros, A. L.; Rosen, M. *Phys. Rev. Lett.*, **1997**, *78*, 1110.
31. Link, B. S.; Mohamed, M.; El-Sayed, M. *J. Phys. Chem. B*, **2001**, *105*, 12286.
32. Shim, M.; Wang, C.; Guyot-Sionnest, P. *J. Phys. Chem. B*, **2001**, *105*, 2369.
33. Kuno, M.; Fromm, D. P.; Johnson, S. T.; Gallagher, A.; Nesbitt, D. J. *Phys. Rev. B*, **2003**, *67*, 125304.
34. Shimizu, K. T.; Neuhauser, R. G.; Leatherdale, C. A.; Empedocles, S. A.; Woo, W. K.; Bawendi, M. G. *Phys. Rev. B*, **2001**, *63*, 205316.
35. Tang, J.; Marcus, R. A. *J. Chem. Phys.*, **2005**, *123*, 054704.
36. Margolin, G.; Barkai, E. *J. Chem. Phys.*, **2004**, *121*, 1566.
37. Frantsuzov, P. A.; Marcus, R. A. *Phys. Rev. B*, **2005**, *72*, 155321.
38. Pelton, M.; Smith, G.; Scherer, N. F.; Marcus, R. A. *Proc. Natl. Acad. Sci. U. S. A.*, **2007**, *104*, 14249.
39. Glennon, J. J.; Tang, R.; Buhro, W. E.; Loomis, R. A. *Nano Lett.*, **2007**, *7*, 3290.
40. Glennon, J. J.; Buhro, W. E.; Loomis, R. A. *J. Phys. Chem. C*, **2008**, *112*, 4813.

41. Kim, H.-H.; Song, N. W.; Park, T. S.; Yoon, M. *Chem. Phys. Lett.*, **2006**, *432*, 200.
42. Gensch, T.; Bohmer, M.; Armendia, P. F. *J. Phys. Chem. A*, **2005**, ***109***, 6653.
43. Jeon, K.-S.; Oh, S.-D.; Suh, Y. D.; Yoshikawa, H.; Masuhara H.; Yoon, M. *Phys. Chem. Chem. Phys.*, **2009**, *11*, 534-542
44. Jang, J. H.; Jeon, K.-S.; Oh, S.; Kim, H.-J.; Asahi, T.; Masuhara, H.; Yoon, M. *Chem. Mater.*, **2007**, *19*, 1984.
45. Hosono, H. *Chem. Lett.* **1997**,523.
46. Kind, H.; Yan, H.; Law, M.; Messer, B.; Yang, P. *Adv. Mater.* **2002**, *14*, 158.
47. Law, M.; Kind, H.; Kim, F.; Messer, B.; Yang, P. *Angew. Chem.* **2002**, *41*, 24505.
48. Bagnall, D. M.; Chen, Y. F.; Zhu, Z.; Yao, T.; Koyama, S.; Shen, M. Y.; Goto, T. *Appl. Phys. Lett.* **1997**, *70*, 2230.
49. Pan, Z.W.; Dai, Z. R.; Wang, Z. L. *Science* **2001**, *291*, 1947.
50. Johnson, J. C.; Yan, H.; Yang, P.; Saykally, R. J. *J. Phys. Chem. B* **2003**,*107*, 8816.
51. Lee, J.; Yoon, M. *J. Phys. Chem. C* **2009**, *113*, 11952.
52. Lee, J.; Choi, S.; Bae, S. J.; Yoon, S. M.; Choi, J. S.; Yoon, M. **2013***, Submitted.*